Understanding the Impact of Nanoflare Heating Frequency on the Observed Emission Measure Distribution

Will T. Barnes, Peter J. Cargill, & Stephen J. Bradshaw

Department of Physics and Astronomy, Rice University
Space and Atmospheric Physics, The Blackett Laboratory, Imperial College London
School of Mathematics and Statistics, University of St. Andrews

Introduction

- Nanoflare model of Parker [11]: corona heated by impulsive ($\ll \tau_{cool}$), low-energy (10^{24} erg) events produced by twisting, braiding of field lines rooted in the photosphere
- "Smoking gun" of nanoflare heating is the faint, high-temperature component of the emission measure distribution, $\mathrm{EM}(T)$ [5, 8]
- While "hot" (i.e. $> 10^{6.6}$ K) part of $\mathrm{EM}(T)$ poorly constrained observationally [14], measurements of the cool ($10^6 < T < 10^{6.6}$ K) part of $\mathrm{EM}(T)$ in AR cores are consistent with loop models heated by intermediate frequency nanoflares [12, 6].
- Fundamental question: what is the frequency of energy release in the solar corona? Two extreme cases:
  - Low-frequency heating: Time between successive events is much greater than typical loop cooling time (i.e. approaches single nanoflare case)
  - High-frequency heating: Time between successive events is much smaller than typical loop cooling time (i.e. approaches steady heating case)
- **Goal:** Use hydrodynamic loop models to better understand how different heating properties, including the heating frequency, affect the "hot" part of the emission measure distribution.

Hydrodynamic Modeling

- Zero-dimensional Enthalpy-based Thermal Evolution of Loops (EBTEL) model of Klimchuk et al. [10], Cargill et al. [7] allows for efficient modeling of many thousands of loops
- We use a modified form of the EBTEL model to treat the electron and ion populations separately [for more details, see 1, submitted]
- Applying the "EBTEL method" to the two-fluid hydrodynamic equations [as given in 3], the modified two-fluid EBTEL equations are,

$$\frac{d}{dt}\bar{p}_e = \frac{\gamma-1}{L}\left[\psi_{TR} - (\mathcal{R}_{TR} + \mathcal{R}_C)\right] + k_B\bar{n}\nu_{ei}(\bar{T}_i - \bar{T}_e) + (\gamma-1)\bar{Q}_e, \tag{1}$$

$$\frac{d}{dt}\bar{p}_i = -\frac{\gamma-1}{L}\psi_{TR} + k_B\bar{n}\nu_{ei}(\bar{T}_e - \bar{T}_i) + (\gamma-1)\bar{Q}_i, \tag{2}$$

$$\frac{d}{dt}\bar{n} = \frac{c_2(\gamma-1)}{c_3\gamma L k_B \bar{T}_e}\left(\psi_{TR} - F_{ce,0} - \mathcal{R}_{TR}\right), \tag{3}$$

where $c_1 = \mathcal{R}_{TR}/\mathcal{R}_C$, $c_2 = \bar{T}/T_a = 0.9$, $c_3 = T_0/T_a = 0.6$, ψ_{TR} is a term included to maintain charge and current neutrality, and ν_{ei} is the electron-ion binary Coulomb collision frequency

- Assume quasi-neutrality, $n_e = n_i = n$, and closed by equations of state: $p_e = k_B n T_e$ and $p_i = k_B n T_i$

Single-nanoflare Results

- Single nanoflare is the most extreme low-frequency case, loop allowed to undergo complete heating and cooling cycle
- In Barnes et al. [1, submitted], we investigated the effect of pulse duration (τ), heat flux limiting, electron versus ion heating, and non-equilibrium ionization (NEI) on the resulting emission measure distribution, $\mathrm{EM}(T)$
- We found that,
  - While very short pulses ($\tau = 20, 40$ s) lead to significant emission above 10 MK, comparisons with field-aligned models [e.g. HYDRAD, 3] show that EBTEL gives an artifically fast rise in density and thus an excess of hot emission for these very short heating times; longer pulses ($\tau = 200, 500$ s) show a cutoff near 10 MK.
  - Compared to pure Spitzer thermal conduction, heat flux limiting (using $f = 1/6$) extends $\mathrm{EM}(T)$ to > 10 MK; extreme values of f (e.g. $f = 1/30$) lead to significant emission > 20 MK.
  - For the case in which the ions are heated, no emission is visible above 8 MK, independent of the pulse duration
  - Including effects due to NEI shows that, even for very short pulses, there is little to no emission visible above 10 MK, for the single-fluid, electron heating, and ion heating cases
- Conclusion: $\mathrm{EM}(T)$ signature of loop plasma heated by a single nanoflare is most likely found in the temperature range $T_m < T < 10^7$ K, where the temperature of maximum emission $T_m \approx 4$ MK for active region (AR) cores [13]

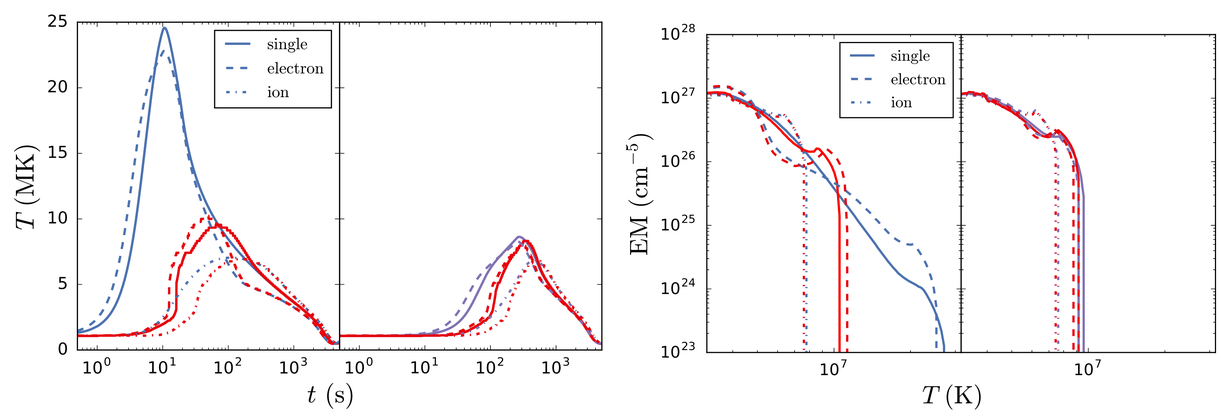

Figure 1: Equilibrium and non-equilibrium (red) ionization results for a single nanoflare lasting 20 s (blue) and 500 s (purple) in the single-fluid case (solid) as well as the case in which only the electrons (dashed) or only the ions (dot-dashed) are heated. **Left:** the electron temperature as a function of time for a 20 s pulse (left) and a 500 s pulse (right). **Right:** corresponding $\mathrm{EM}(T)$ for the equilibrium (left, blue and right, purple) and NEI (red) cases.

Energy Budget and Heating Statistics

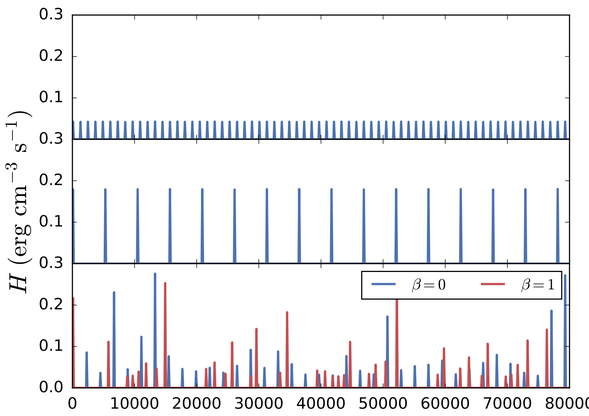

Figure 2: Top (Middle) panel shows Uniform heating amplitudes for $t_N = 1000$ ($t_N = 5000$) s. Bottom panel shows Heating amplitudes drawn from a power-law distribution with $\alpha = -1.5$ and mean wait time $t_N = 2000$ s; the events shown in red (blue) have wait times that depend on the previous event energy (uniform wait times).

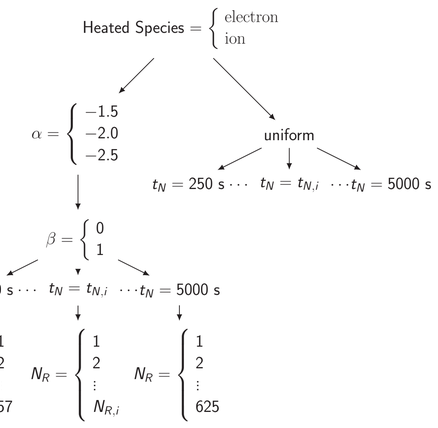

Figure 3: Heating function parameter space. We consider a range of waiting times $250 < t_N < 5000$ s, in increments of 250 s. In the power-law case, a sufficiently large number of runs, N_R is required to sample the distribution. For example, when $t_N = 5000$ s, $N_R = 625$ such that for each $(\alpha, \beta, t_N = 5000)$, we run the model 625 times.

- Loop of half-length $L = 40$ Mm heated by N triangular pulses with duration $\tau = 200$ s over $t_{total} = 8 \times 10^4$ s.
- Each event has maximum heating rate H_i and followed by a waiting time of $t_{N,i}$; static background heating $H_{bg} = 3.5 \times 10^{-5}$ erg cm^{-3} s^{-1}
- H_i can either be uniform such that $H_i = H_0$ for all i or chosen from a power-law distribution with $\alpha = -1.5, -2.0, -2.5$
- The total energy injected into the loop is constrained by,

$$H_{eq} = \frac{1}{t_{total}}\sum_{i=1}^{N}\int_{t_i}^{t_i+\tau} \mathrm{d}t\ Q(t) = \frac{\tau}{2t_{total}}\sum_{i=1}^{N} H_i, \tag{4}$$

- $H_{eq} \approx 3.6 \times 10^{-3}$ erg cm^{-3} s^{-1} is the time-averaged heating rate such that $T_m \approx 4$ MK, consistent with AR core observations [13].
- Treat $t_{N,i}$ as time needed for the field to "unwind", consistent with the Parker [11] nanoflare picture
  - $\beta = 0$: $t_{N,i} = t_N$ for all i, no dependence on H_i
  - $\beta = 1$: $\varepsilon = LA\tau H_i/2 \propto t_{N,i}$ (see bottom panel of Fig. 2)
- Total number of events dependent on t_N, $N = t_{total}/(t_N + \tau)$ such that $N = 16$ when $t_N = 5000$ s
- For the power-law cases, require $NN_R \sim 1 \times 10^4$, where N_R is the number of runs for each unique point in the parameter space, (α, β, t_N)

Emission Measure Distribution

- Compute solutions to Eqs. 1, 2, and 3 for all N_R runs for each point in the multidimensional heating parameter space. (Note: for the events of uniform magnitude, $N_R = 1$)
- To account for NEI, we use the numerical code described in Bradshaw [2] to calculate the fractional ionization states for Fe IX through Fe XXVII and calculate T_{eff}, a temperature that would be measured based on the actual ionization states
- Given a temperature range $4 \leq \log T_e \leq 8.5$ with bin widths $\Delta \log T_e = 0.01$, at each time t_j, add $n_j^2(2L)$ to every bin that falls in the range $[T_{0e,j}, T_{ae,j}]$; time-averaging over the entire run gives $\mathrm{EM}(T)$
- To calculate $\mathrm{EM}(T_{eff})$, we use the same procedure, but using T_{eff} instead of T_e.

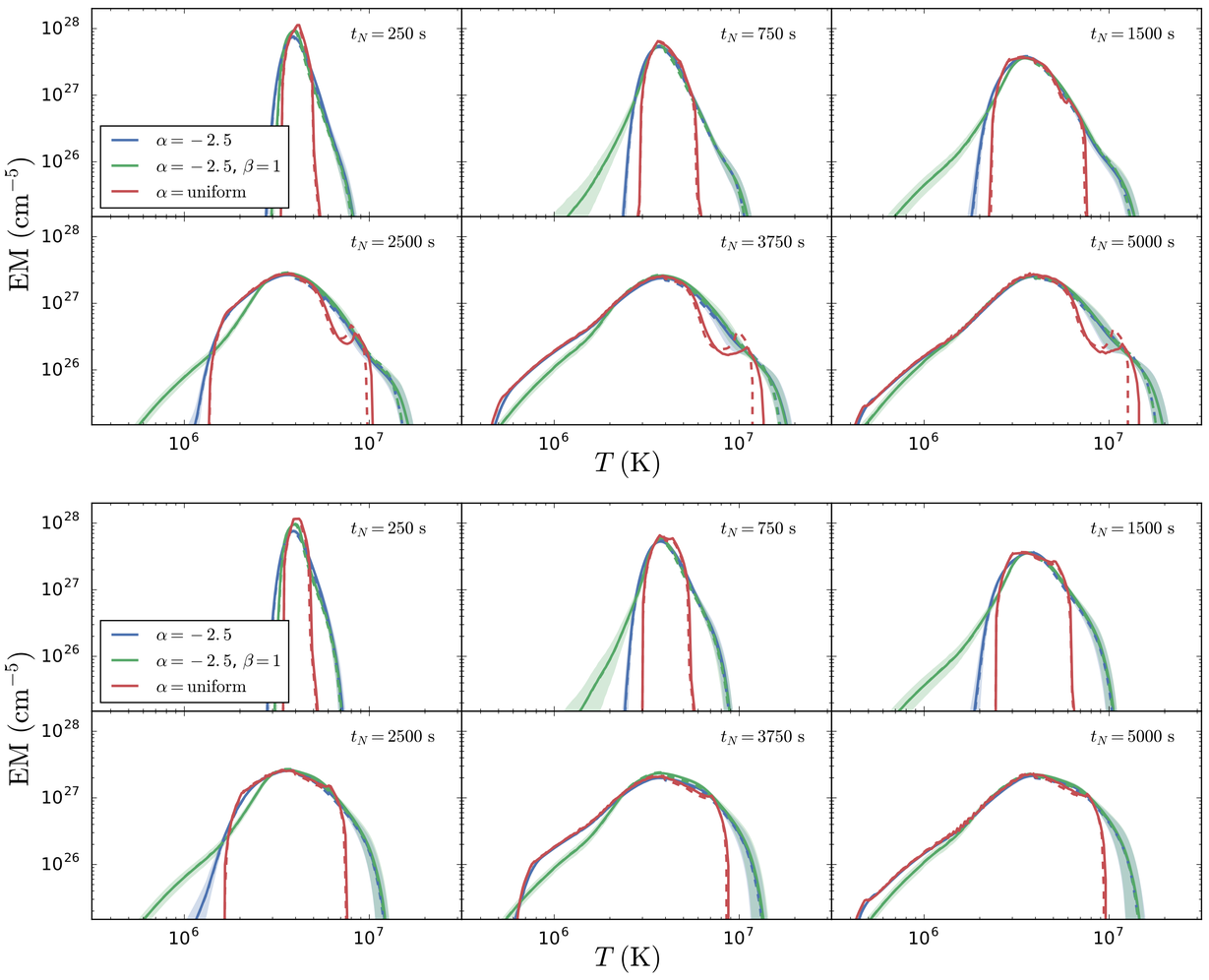

Figure 4: Emission measure distributions for waiting-times $t_N = 250, 750, 1500, 2500, 3750, 5000$ s in the electron (top) and ion (bottom) heating cases. The three types of heating functions shown are uniform heating rates (red), heating rates chosen from a power-law distribution of $\alpha = -2.5$ (blue), and heating rates chosen from a power-law distribution of $\alpha = -2.5$ where the time between successive events is proportional to the heating rate of the preceding event (green). The solid lines in the two power-law cases show the mean $\mathrm{EM}(T)$ over N_R runs and the shading indicates 1σ from the mean. The dashed lines denote the corresponding $\mathrm{EM}(T_{eff})$ distribution. The standard deviation is not included in the NEI results.

Hot Plasma Diagnostics

- Well-known cool emission measure scaling $\mathrm{EM}(T) \propto T^a$; similar scaling claimed for the hot part of the emission measure distribution, $\mathrm{EM}(T) \propto T^{-b}$ over a temperature range $T_m \lesssim T \lesssim 10^{7.2}$.
- Observations have shown $7 \lesssim b \lesssim 10$ [13] though measurements of b are poorly constrained due to lack of spectroscopic data in this temperature range; b very sensitive to the temperature range over which the fit is performed.
- Brosius et al. [4] find the ratio of Fe XIX (formed at $T \approx 10^{6.95}$ K) to Fe XII (formed at $T \approx 10^{6.2}$ K) intensity to be ~ 0.59 inside AR core compared to ~ 0.076 outside, providing possible evidence for impulsive heating.
- As a proxy for this intensity ratio and an alternative to b, we compute an emission measure ratio $\mathrm{EM}(T_{hot})/\mathrm{EM}(T_{cool})$, with $T_{hot} = 10^{6.95}$ K and $T_{cool} = 10^{6.3} \approx 2 \times 10^6$ K.

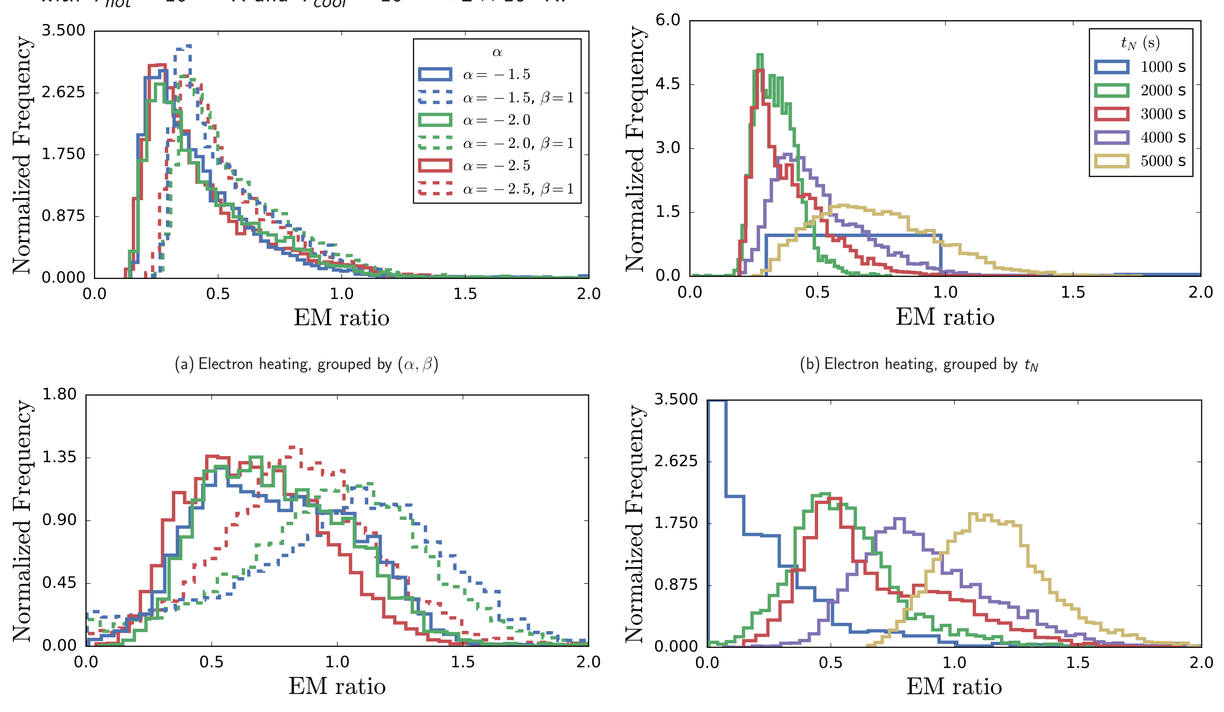

(a) Electron heating, grouped by (α, β)

(b) Electron heating, grouped by t_N

(c) Ion heating, grouped by (α, β)

(d) Ion heating, grouped by t_N

Figure 5: Histograms of emission measure ratios for the entire multidimensional heating parameter space (see Fig. 3). Each histogram is normalized such that for each distribution $P(x)$, $\int_{-\infty}^{\infty} \mathrm{d}x\, P(x) = 1$ and the bin widths are calculated using the well-known Freedman-Diaconis formula [9]. The top panels show the electron heating cases and the bottom panels show the ion heating cases. In the left panels, each histogram (denoted by linestyle and color) corresponds to a unique heating function (α, β). The uniform case has not been included here. In the right panels, the emission measure ratios are grouped by t_N. Here we show only five values of t_N for aesthetic reasons.

Conclusions

- While cool part of $\mathrm{EM}(T)$ more elongated for $\beta = 1$, hot part of emission measure distribution independent of β.
- For intermediate heating frequencies, power-law cases (compared to uniform case) show significantly more hot emission, for both electron and ion heating
- Compared to single-nanoflare results, ion heating results show $\mathrm{EM}(T)$ extending to hotter temperatures ($> 10^7$ K) for intermediate to low heating frequencies
- Effects due to NEI only important for uniform heating in electron heating case, no visible differences in ion heating case
- Emission measure ratio seems to be largely independent of α, weakly dependent on β.
- In ion heating case, lower t_N required for consistency with Brosius et al. [4] results as compared to electron heating case.

References

[1] Barnes, W. T., Cargill, P. J., & Bradshaw, S. J. 2016, submitted
[2] Bradshaw, S. J. 2009, Astronomy and Astrophysics, 502, 409
[3] Bradshaw, S. J., & Cargill, P. J. 2013, The Astrophysical Journal, 770, 12
[4] Brosius, J. W., Daw, A. N., & Rabin, D. M. 2014, The Astrophysical Journal, 790, 112
[5] Cargill, P. J. 1994, The Astrophysical Journal, 422, 381
[6] —. 2014, The Astrophysical Journal, 784, 49
[7] Cargill, P. J., Bradshaw, S. J., & Klimchuk, J. A. 2012, The Astrophysical Journal, 752, 161
[8] Cargill, P. J., & Klimchuk, J. A. 2004, The Astrophysical Journal, 605, 911
[9] Freedman, D., & Diaconis, P. 1981, Zeitschrift fr Wahrscheinlichkeitstheorie und Verwandte Gebiete, 57, 453
[10] Klimchuk, J. A., Patsourakos, S., & Cargill, P. J. 2008, The Astrophysical Journal, 682, 1351
[11] Parker, E. N. 1988, The Astrophysical Journal, 330, 474
[12] Reep, J. W., Bradshaw, S. J., & Klimchuk, J. A. 2013, The Astrophysical Journal, 764, 193
[13] Warren, H. P., Winebarger, A. R., & Brooks, D. H. 2012, The Astrophysical Journal, 759, 141
[14] Winebarger, A. R., Warren, H. P., Schmelz, J. T., et al. 2012, The Astrophysical Journal Letters, 746, L17

This work was supported in part by the Big-Data Private-Cloud Research Cyberinfrastructure MRI-award funded by NSF under grant CNS-1338099 and by Rice University.

wtbarnes

Mail: will.t.barnes@rice.edu